Retraction for *RSC Advances*:

Aligned nanoporous PtNi nanorod-like structures for electrocatalysis and biosensing

Huajun Qiu, Liang Li, Qiaolin Lang, Feixue Zou and Xirong Huang

RSC Adv., 2012, 3548–3554 (DOI: 10.1039/C2RA01308H). **Retraction published 26 September 2012**

We, the named authors, hereby wholly retract this *RSC Advances* article, due to unreliable experimental results which cannot be repeated.

Signed: Huajun Qiu, Liang Li, Qiaolin Lang, Feixue Zou and Xirong Huang, China, September 2012

Retraction endorsed by Sarah Ruthven, Managing Editor.

PAPER

Aligned nanoporous PtNi nanorod-like structures for electrocatalysis and biosensing†

Huajun Qiu,[*ac] **Liang Li,**[b] **Qiaolin Lang,**[b] **Feixue Zou**[a] **and Xirong Huang**[a]

We describe the one-step dealloying of PtNiAl ternary alloy to fabricate aligned nanoporous PtNi (np-PtNi) nanorod-like structures with predetermined alloy composition. Electron microscopy and X-ray diffraction characterizations demonstrate that the selective etching of Al from PtNiAl alloy with multiphases generates aligned np-PtNi alloy nanorods. The formation of nanoporous nanorod-like structures with uniform PtNi alloy ligament should be due to the fast diffusion, self assembly and strong interaction between Pt and Ni during the dealloying process. With the ligament size less than 5 nm, the np-PtNi nanorods exhibit remarkably improved electrocatalytic activity towards ethanol oxidation and H_2O_2 oxidation/reduction compared with the commercial Pt/C catalyst. When coupled with glucose oxidase, the enzyme modified np-PtNi electrode can sensitively detect glucose over a wide linear range (0.5–21 mM).

Introduction

Due to the unique properties of nanomaterials (electronic, optical, magnetic and catalytic), fabrication of novel nanostructured materials and studying their applications in sensing/biosensing have attracted much attention in recent years. Particularly, noble metal (such as Pt) nanomaterial-based electroanalytical chemistry has continued to receive considerable interest due to the high electrocatalytic activity of Pt, rapid detection, and high sensitivity.[1] These Pt-based nanomaterials can also be further functionalized with biocatalyst (enzyme) for wider electroanalytical applications by combining the electrocatalytic activity of Pt nanomaterials and the biocatalytic activity of enzymes. For example, Pt nanoparticle-glucose oxidase hybrid has been used for glucose biosensing through electrochemical determination of H_2O_2 produced by the enzymatic reaction.[2–4] It is known that pure Pt can be easily poisoned by CO and the addition of a second metal, such as Ru, Au, Ni, *etc.*, can improve its tolerance to poisoning and the overall catalytic activity. Therefore, Pt-based bimetallic nanostructures (especially alloyed with non-precious metals such as Ni) have been widely studied.[5–12] It has also been demonstrated that the catalytic activity of metal nanomaterials are also relative to their morphology, size, bimetallic composition, *etc.* Great efforts have been dedicated toward the construction of

functional Pt-based nanostructures with various morphologies, ultrafine particle size, and predetermined bimetallic ratio in order to achieve higher catalytic activity and better utilization of Pt. These bimetallic nanostructures with various morphologies are usually in the form of alloys, core/shell structures, and heteroaggregates.[13–22]

Metal nanorods/nanowires (especially aligned nanorods/nanowires with hollow interiors or tailored porosity) have attracted wide interest due to their intriguing physicochemical properties, and are applicable in important fields including catalysis,[23] biological labeling,[24] surface-enhanced Raman scattering,[25–27] electrogenerated chemiluminescence,[28,29] *etc.* For the fabrication of these one-dimensional nanostructures, template-based synthesis is one of the most widely used routes.[30–33] For example, AuAg alloy nanorods have been prepared by electrodeposition using porous alumina as the template, and then the AuAg nanorods are chemically/electrochemically dealloyed to obtain nanoporous gold nanorods.[30,33] The same strategy has also been used for the fabrication of nanoporous PtCo and PtNi nanowires.[23,34] In another fabrication strategy, dispersed (not aligned) nanoporous gold nanowires can be obtained by galvanic replacement reaction between Ag nanowires and $HAuCl_4$ at a high temperature of 100 °C.[35] However, these methods require template preparation and removal (porous alumina template) or the excessive use of surfactants and high temperatures (Ag nanowire template). Moreover, these methods are not quite suitable for large scale fabrication.

Recently, dealloying, which refers to selective dissolution of one or more components out of an alloy, has been demonstrated to be an ideal method to fabricate three-dimensional (3D) nanoporous metals with bicontinuous ligament/pore structure.[36–42] Nanoporous metals prepared by dealloying have some

[a]School of Chemistry and Chemical Engineering, Shandong University, Jinan, 250100, China
[b]Qingdao Institute of Bioenergy and Bioprocess Technology, Chinese Academy of Sciences, Qingdao, 266101, China
[c]School of Chemical and Biomedical Engineering, Nanyang Technological University, 70 Nanyang Drive, Singapore 637457.
E-mail: qiuhuajun@gmail.com
† Electronic supplementary information (ESI) available: See DOI: 10.1039/c2ra01308h

unique properties such as adjustable pore/ligament size, excellent electron conductivity, extremely clean ligament surface, *etc.* and have been widely investigated in applications such as catalysis, sensing, SERS, and so forth.[25,27,38,43–52] It is generally recognized that ideal bicontinuous nanoporous structures are obtained from dealloying binary alloys with a single phase solid solubility across all compositions (like AuAg alloy).[36] In comparison with the single phase alloy system, less attention has been paid to the dealloying of two-phase or multiphase alloy systems and the resulting products. In theory, for a two-phase system, if one phase can be dealloyed and another not, a two phase alloy can be used to fabricate porous/nonporous metal composites. If the two phases can be separately dealloyed, then nanoporous metal composite with two kinds of nanoporous metals or two different pore size distributions can be obtained. For example, by dealloying AuAl alloy which contains Al_2Au and AlAu phases, nanoporous gold with two pore size distributions can be obtained.[42] If one phase is entirely removed and another is dealloyed, the dealloying of the two phase alloy leads to nanoporous metals with bimodal channel/pore size distributions.[40] The big channels are formed by the entire removal of one metal phase; while, the small channels/pores result from the selective dissolution of an alloy phase. However, what can we obtain if multiphase alloy systems are dealloyed? The multiphase system may contain metal phase which can be completely removed and different alloy phases which can be selectively dealloyed. In the present work, we report that by one-step dealloying PtNiAl ternary alloy containing multiple alloy phases in NaOH solution, aligned np-PtNi alloy nanorod-like structures can be successfully fabricated. The mechanism of the formation of aligned nanorods is discussed. Moreover, the aligned np-PtNi nanorods have greatly enhanced electrocatalytic activity and sensing performance towards some small molecules such as alcohols and hydrogen peroxide. After being loaded with glucose oxidase (GOx), a sensitive glucose biosensor is also fabricated.

Experimental

Reagents

GOx from *Aspergillus niger* was purchased from Sigma-Aldrich. H_2O_2 solution (30%) and D-(+)-glucose were purchased from Sinopharm Chemical Reagent Co., Ltd. Commercial Pt/C (10 wt.% on carbon, a Johnson Matthey Company product) was purchased from Alfa Aesar. Other chemicals were of analytical grade. $Pt_{13}Ni_7Al_{80}$ (at.%) alloy foil with thickness of ~ 50 μm was prepared by refining high-purity (>99.9%) Pt, Ni and Al in a high-frequency induction furnace. Using a single roller melt spinning apparatus, the pre-alloyed ingot was re-melted by high-frequency induction heating in a quartz tube and then melt-spun onto a copper roller with a diameter of 0.35 m at a speed of 1000 revolutions per minute (rpm) under nitrogen-protected atmosphere.

Apparatus

X-Ray diffraction (XRD) analysis was carried out on a Bruker D8 advanced X-ray diffractometer using Cu KR radiation at a step rate of $0.04°$ s^{-1}. The morphologies of the samples were characterized by a JEM-2100 transmission electron microscope

(TEM) and a JSM-6700 field-emission scanning electron microscope (SEM) equipped with an Oxford INCA x-sight energy dispersive X-ray spectrometer (EDS). Surface states were analyzed with an ESCALab250 X-ray photoelectron spectroscopy (XPS). Electrochemical measurements were performed on a CHI760C potentiostat in a three-electrode cell with a nanoporous nanorod electrode as working electrode, a Pt foil as counter electrode and a saturated mercurous sulfate electrode as reference electrode. All the potentials given in this paper were *vs.* reversible hydrogen electrode (RHE). CO stripping experiments were carried out by first holding the electrodes at 0.15 V in 0.5 M H_2SO_4 solution with continuous CO bubbling for 20 min. The electrode was then transferred into a 0.5 M N_2-purged H_2SO_4 solution to record the CO stripping profiles.

Preparation of the np-PtNi nanorods

np-PtNi nanorods were prepared by dealloying the as-prepared PtNiAl ternary alloy foil in 1 M NaOH solution for 24 h at room temperature, followed by rinsing thoroughly with pure water. The monolithic nanoporous nanorod foil was used as the working electrode and the substrate for GOx immobilization.

Preparation of the GOx/nanoporous nanorod biosensor

The GOx modified nanoporous nanorod electrode was made by dropping 4 μL GOx stock solution (5 mg mL^{-1}) on the electrode. After dried at 4 °C, 2 μL Nafion (0.5 wt.%) was coated to avoid enzyme leakage.

Results and discussion

Preparation and characterization of aligned np-PtNi nanorod-like structure

Considering the active property and rich supply of Al, Al-based ternary alloy is chosen as the precursor alloy. The atomic percentage (at.%) of Al is set at 80%. Based on previous reports for PtNi alloy electrocatalysts, the optimal at.% of Ni is usually in the range from 30 to 40 at.%,[5,53] in this work the at.% of Pt and Ni in the ternary alloys are controlled to be 13% and 7%, respectively. Thus, the content of Ni in the resulted PtNi alloy is 35 at.% after the removal of Al from the $Pt_{13}Ni_7Al_{80}$ alloy in 1.0 M NaOH aqueous solution (a detailed study on the effect of Ni content is not included in this work). EDS characterization (Fig. S1a in the ESI†) of the ternary precursor alloy demonstrates that the ratio of the three components is almost the same as the initial feed ratio. After 24 h dealloying, EDS result shows that Al is etched to an undetectable level while the content of Pt and Ni is unchanged (Fig. S1b, ESI†).

XRD is used to examine the phase structures of the PtNiAl ternary alloy and the dealloyed sample (Fig. S2, ESI†). For the ternary alloy, due to the large content of Al, a pure Al phase exists. The other diffraction peaks are complex and can be ascribed to different Al-based alloy phases such as Al_3Ni, Al_6Pt, Al_3Ni_2, *etc.* indicating the existence of multiple alloy phases in the precursor alloy. However, it is interesting to find that after the 24 h dealloying, accompanied with the complete removal of Al, a uniform PtNi alloy structure is obtained. One can see from Fig. S2 (ESI†) that the dealloyed sample shows a set of three diffraction peaks which are assigned to the (111), (200), (220)

reflections of face-centered cubic structure. No peaks from pure Ni (or its oxides) as well as Pt-Ni ordered alloy phase are observed, which suggests the formation of disordered single-phase PtNi alloy. As compared with the standard diffraction pattern of Pt, all diffraction peaks for the dealloyed sample shift to higher angles due to the substitution of smaller Ni atoms in Pt crystal lattice. Notably, the diffraction peak from (111) diffraction are more pronounced, while those from (200) and (220) diffraction are so weak that they are barely discernible. This indicates that the PtNi alloy is primarily dominated by (111) facets.

Fig. 1a and 1b show the plan-view and section-view, respectively, of SEM images of the dealloyed sample. It can be observed that the resulted sample consists of well-aligned nanorod-like structures with a diameter of 200–500 nm (Fig. 1a) and a length of over 1 μm (Fig. 1b). Fig. 1c is the enlarged SEM image of the nanorods, which shows bicontinuous ligament-pore structure with the ligament size of ∼3 nm. The clear contrast between the dark skeletons and inner bright pores in the TEM image (Fig. 1d) further indicates the formation of an open interconnected network structure within each nanorod. HRTEM image (Fig. 1e) provides more details for this structure, in which the continuous lattice fringes are well resolved around the whole pore, indicating the formation of single-crystalline interconnected ligaments. It is noted that most of the exposed facets are along (111) planes with the lattice spacing measured to be 0.215 nm which is in accordance with the value calculated by Vegard's law. The result that most exposed facets are along (111) planes is also in excellent agreement with that obtained from the XRD study.

XPS is further used to examine the surface properties of np-PtNi. Fig. S3a in the ESI† shows the Ni 2p spectrum of np-PtNi nanorods. The spectrum shows the presence of metal Ni as well as Ni oxide and hydroxides (NiO, Ni(OH)$_2$, and NiOOH). The Ni 2p spectrum shows a complex structure with an intense satellite signals at high binding energy adjacent to the main peaks, which can be attributed to multielectron excitation.[5] The Ni 2p XPS peaks at the binding energies of 852.7, 853.8, 855.6, and 857.3 eV correspond to Ni^0, NiO, Ni(OH)$_2$, and NiOOH, respectively [5]. Fig. S3b in the ESI† presents the XPS spectra of the Pt 4f region for the np-PtNi nanorods. The two peaks can be ascribed to metal Pt and no signals related to oxidized Pt species are observed. The electronegativity difference between Ni and Pt (1.9 and 2.2, respectively) implies an electron-withdrawing effect of Pt from the neighbouring Ni atoms, which makes the latter more difficult to reduce.

It is very interesting to find that by a simple dealloying of PtNiAl alloy, aligned nanoporous nanorod-like structure with uniform PtNi alloy ligament can be successfully fabricated. The dealloying process has been widely studied in previous work. Most of these studies are focused on dealloying of binary alloy such as AgAu alloy for the preparation of nanoporous gold (NPG).[54] The formation mechanism has been discussed according to corrosion disordering/diffusion reordering model, dynamic roughening transition model and kinetic Monte Carlo model.[55,56] However, in the present case, for the PtNiAl ternary alloy with multiple alloy phases, the dealloying process and formation mechanism of the aligned nanoporous nanorod-like structure are obviously more complicated. We assume that the dealloying of the ternary alloy started firstly with the pure Al phase (the most active component). The removal of pure Al phase would result in the formation of the large channels in the alloy. The formed large channels also facilitate the diffusion of the dealloying solution and the further dealloying of AlNi and AlPt alloy phases. Accompanied with the removal of Al in the AlNi and AlPt alloy phases, the remaining Ni and Pt adatoms on the alloy/solution interface will interdiffuse to form PtNi alloy ligaments and nanopores. It is reasonable to believe that these different Al-based alloy phases should be very close to each other and the interdiffusion and interaction between the left Pt and Ni must be very strong, which results in the formation of uniform PtNi alloy instead of hybrid of nanoporous Pt and nanoporous
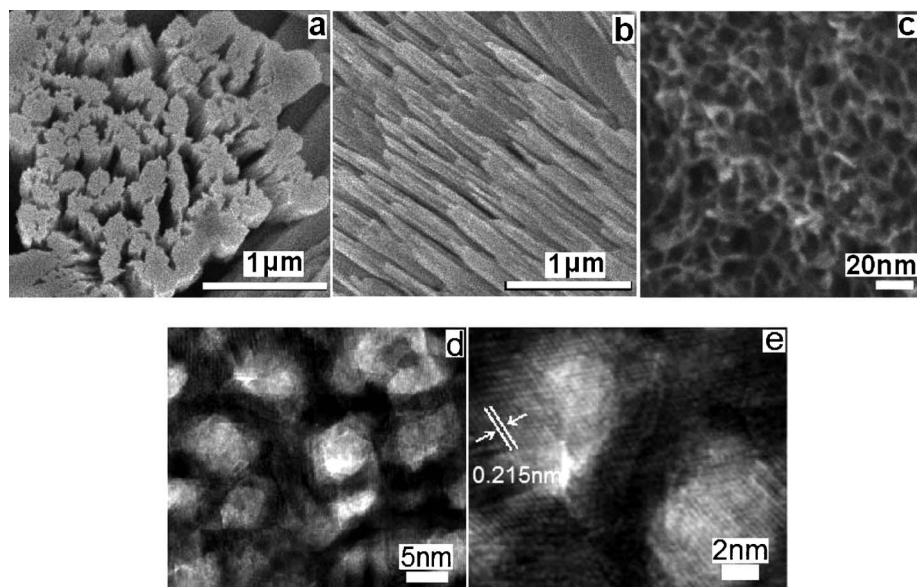
Fig. 1 SEM images of np-PtNi nanorod-like structure [plan-view, (a); section-view, (b); enlarged SEM image, (c)], TEM (d) and HRTEM (e) images of the sample.

Ni. To explain the formation of nanorod-like structures, due to the coexistence of multiple alloy phases, it is assumed that as the pure Al phase is etched away the remaining Al-based alloy phases might also go through a fast self-assembly process to form aligned nanorod-like structures. On the other hand, it is quite possible that in the precursor PtNiAl alloy, these Al-based alloy phases exist in the form of nanorods and after the dealloying, the nanorod-like structure is maintained. The exact mechanism still needs further investigation.

Electrocatalytic properties of np-PtNi

Direct ethanol fuel cells have been attracting enormous attention as power sources since ethanol is environmentally-friendly and can be easily produced in large quantities through a green fermentation process. On the other hand, ethanol sensing is very important for medicine, brewing and beverages, *etc.* Therefore, developing an anode catalyst with high electrocatalytic activity towards ethanol oxidation is significant. In the present work, for the evaluation of the electrocatalytic activity and electroanalytical performance of np-PtNi nanorods, the state-of-the-art commercial Pt/C catalyst is used for comparison and all current densities are normalized by the real electrochemical active surface area (EASA) of Pt calculated by integrating the charge associated with H desorption.[57]

Fig. 2a shows the cyclic voltammograms (CVs) of np-PtNi and Pt/C catalyst in 0.5 M H_2SO_4 + 1.0 M ethanol solution. It is observed that the anodic peak in the forward scan locate at 0.90 V for np-PtNi, which is much lower than that of the Pt/C catalyst (0.95 V), indicating more favorable ethanol oxidation on the alloy nanorod electrode. More importantly, the specific current density of np-PtNi is about 2.5 times that of Pt/C. To explain the enhanced electrocatalytic activity of np-PtNi, the presence of Ni oxygenated species on np-PtNi surface would provide rich oxygen source for CO_{ads} oxidation during alcohol electrooxidation and leave the active sites of Pt for further reaction (*i.e.*, bifunctional mechanism).[5] The electronic structure modification of Pt by the interaction with Ni (demonstrated by the XPS study) should also contribute to the enhancement. Moreover, compared with Pt/C catalyst, the 3D bicontinuous spongy structure within each nanorod provides good transport channels for electrons and small molecules, which should

effectively facilitate the reaction kinetics on the nanoporous nanorod electrode.

For ethanol electro-oxidation, two anodic peaks are observed in one potential cycle. The anodic peak in the forward scan is ascribed to the oxidation of freshly adsorbed ethanol molecules on the electrode surface, and usually used for the evaluation of catalyst activity. However, there are still controversies about the origin of the oxidation peak during the backward scan. Some thought that the anodic peak in the backward scan was attributed to the oxidation of incompletely oxidized carbonaceous intermediates accumulated on the catalyst surface during the forward scan.[7] While others believed that the reverse current peak cannot be ascribed to the intermediate species removal, and should originate from the oxidation of the fresh molecules on reduced (re-activated) Pt surface because they experimentally demonstrated that most intermediates are removed when the potential is over 0.6 V *vs.* RHE (using methanol as model).[6] Here, we observe that by increasing the scan rates, the ratio of the forward anodic peak current (I_f) to the backward anodic peak current (I_b) decreases (I_f/I_b is 0.67 at 100 mV s^{-1} and 0.94 at 10 mV s^{-1}, Fig. S4†). It is known that in the forward scan, a faster scan rate usually causes insufficient molecule oxidation producing more intermediates, thus the decreased I_f/I_b with increasing scan rates might be due to more intermediate oxidation in the backward scan. Therefore, the reverse current peak might be indeed related to the oxidation of intermediates. However, the large peak current density in the backward scan cannot exclude the oxidation of fresh alcohol molecules on re-activated Pt surface. It is possible that both the oxidation of intermediates and fresh molecules attribute to the large reverse peak current.

To get more insights into the enhanced electrocatalytic activity of np-PtNi, CO electro-stripping experiment was carried out. As shown in Fig. S5 (ESI†), the CO stripping peak on np-PtNi locates at 0.74 V, which is greatly negatively shifted (by ~100 mV) compared with that on Pt/C (0.83 V). The current density for CO electro-oxidation on np-PtNi is also smaller than that on Pt/C. These results indicate that the CO adsorption is much weaker on the np-PtNi than on Pt/C. In other words, the np-PtNi is much more tolerant to CO poisoning. The weak CO adsorption should be due to the electronic modification of Pt
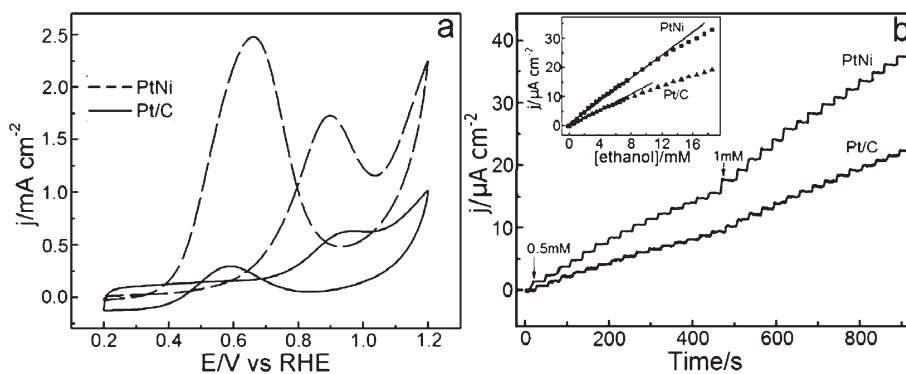
Fig. 2 CVs of np-PtNi and Pt/C electrodes in 0.5 M H_2SO_4 + 1.0 M C_2H_5OH solution, scan rate: 50 mV s^{-1} (a); current responses of np-PtNi and Pt/C electrodes on successive addition of C_2H_5OH in 0.5 M H_2SO_4 solution at 0.9 V (b); inset of (b) is plots of current at 0.9 V *versus* C_2H_5OH concentrations.

through interaction with Ni and the existence of surface Ni oxygenated species.

The analytical performance of np-PtNi is evaluated by recording its amperometric response to successive addition of ethanol into the electrolyte (Fig. 2b). The two electrodes respond quickly and sensitively to each addition of ethanol. The np-PtNi exhibits a much higher sensitivity and wider linear range (up to 16 mM, $R = 0.997$) with the detection limit of ~ 20 μM (inset in Fig. 2b). The enhanced electroanalytical performance of the np-PtNi is clearly due to its higher electrocatalytic activity and better resistance to CO poisoning. This linear range is wider than those of some alcohol dehydrogenase (ADH)-based electrochemical ethanol sensors such as ADH/NPG (1.0–8.0 mM),[43] ADH/carbon nanotubes (CNT) (0.5–5.0 mM)[58] and ADH/ reduced graphene oxide (0.9–10 mM).[59]

In addition to the remarkably increased electrocatalytic activity towards ethanol oxidation, np-PtNi also exhibits enhanced electrocatalytic activity towards the oxidation/reduction of H_2O_2, an essential mediator in food, pharmaceutical, clinical and enzymatic reaction. Fig. 3 shows CVs of np-PtNi and Pt/C electrodes in 0.1 M PBS (pH 7.0) in the presence and absence of 10 mM H_2O_2. It is observed that compared with Pt/C electrode (Fig. 3b), the np-PtNi electrode exhibits both higher oxidation current starting from ~ 0.25 V during the forward scan and higher reduction current starting at ~ 0.53 V during the backward scan in the presence of 10 mM H_2O_2 (Fig. 3a). In particular, it is noted that on Pt/C electrode, the current for H_2O_2 reduction starts at ~ 0.42 V which is ~ 0.11 V negatively shifted compared with that on np-PtNi. The more positive onset potential and much higher current density for H_2O_2 reduction on np-PtNi indicate that the as-prepared nanoporous alloy nanorods have greatly enhanced electrocatalytic activity towards H_2O_2 reduction.

Fig. 4 shows the amperometric responses of the two electrodes on successive addition of H_2O_2 into the stirring PBS at 0.1 V. As observed, the two electrodes respond rapidly to the addition of H_2O_2 and reach the maximum steady-state currents within 4 s. The np-PtNi electrode has a higher current response compared with Pt/C electrode. This result is also in good agreement with the results obtained from the CV study. As shown in the inset of Fig. 4, np-PtNi electrode exhibits linear response to H_2O_2 concentration up to ~ 2.0 mM ($R = 0.996$) with a detection limit of 0.5 μM, which is lower than certain horseradish peroxidase (HRP) and carbon nanotube (CNT)-based biosensors.[60–62] The

reproducibility of the np-PtNi electrode has also been studied. For the same electrode, the relative standard deviations (RSD) for 0.4 mM H_2O_2 are 3.6% for five measurements. For five np-PtNi electrodes, the RSD is 4.6%. The nanoporous nanorod electrode also shows good long-term stability. The electrode was tested for the detection of 1.0 mM H_2O_2 every three days for one month and the current response retained $\sim 95\%$ of the initial value.

The stability of electrocatalysts under long-term electrochemical operation conditions is important for their practical applications as both fuel cells and electrochemical sensors. The structure stability of np-PtNi under long-term continuous potential cycling from 0.6 V to 0.9 V in 0.5 M H_2SO_4 solution was studied by monitoring the change of its EASA (Fig. S6 in ESI†). It is observed that the EASA of Pt/C suffers a significant loss ($\sim 75\%$ remained) after 5000 cycles, while that of the np-PtNi nanorod retains more than 90% of its initial value, indicating that alloying Pt with Ni greatly improves the structure stability.

Electrochemical biosensing

The excellent performance of np-PtNi electrode towards the detection of H_2O_2 makes them attractive for the fabrication of oxidase-based biosensors. GOx is chosen as the model enzyme. The amount of GOx immobilized is first optimized. For 20 mM glucose, a GOx loading of 0.02 mg is appropriate for the quick conversion. Fig. 5 shows the amperometric responses of the two GOx modified electrodes to successive addition of glucose at 0.1 V. It is observed that the GOx/np-PtNi electrode responds quickly (~ 5 s) and more sensitively to each addition of glucose. The calibration curve (inset in Fig. 5) shows that the np-PtNi-based biosensor has a linear response to glucose concentration in the range of 0.5 to 21 mM ($R = 0.997$) with a detection limit of ~ 0.1 mM. The linear range of the present biosensor is also wider than or comparable with that of GOx/NPG (1–18 mM),[43] GOx/CNT/nano-Pt (25 nM-2 mM),[63] GOx/CNT/Teflon (2–20 mM)[61] and GOx/reduced graphene oxide (0.01–10 mM)[59] biosensors. The physiological level of ascorbic acid (0.2 mM) and uric acid (0.02 mM) only have negligible interference at this biosensor, which should be due to the low detection potential and the existence of Nafion membrane acting as an effective permselective barrier.[62] Like the bare np-PtNi, the GOx/np-PtNi also has good reproducibility and long-term stability. For five biosensors
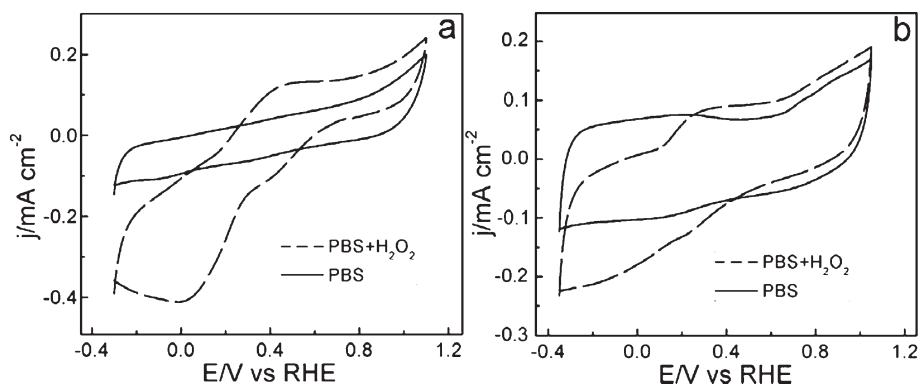
Fig. 3 CVs of np-PtNi (a) and Pt/C (b) electrodes in PBS (0.1 M, pH 7.0) with and without 10 mM H_2O_2, scan rate: 50 mV s^{-1}.
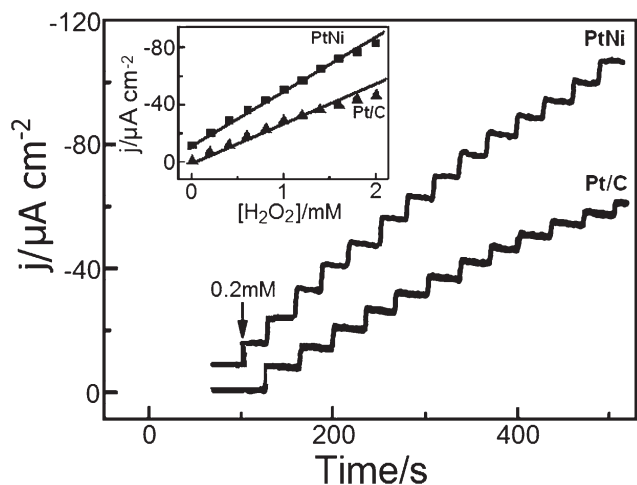
Fig. 4 Amperometric current responses of np-PtNi and Pt/C electrodes on successive addition of H_2O_2 into the stirring PBS (0.1 M, pH 7.0); applied potential: 0.1 V; inset is plots of current *versus* H_2O_2 concentrations.
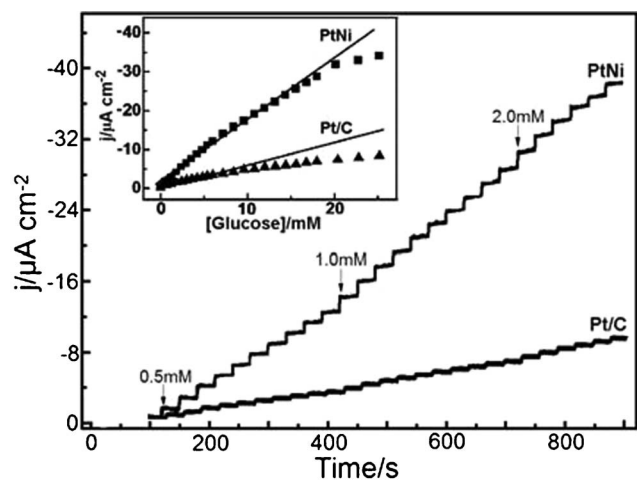
Fig. 5 Amperometric current responses of GOx/np-PtNi and GOx/Pt/C electrodes on successive addition of glucose into the stirring PBS (0.1 M, pH 7.0); applied potential: 0.1 V; inset is plots of current *versus* glucose concentrations.

prepared in the same way, a RSD of 4.7% is obtained when detecting 4 mM glucose. After 1 month storage at 4 °C, the response retains ∼94% of its initial value.

The much higher current response on the GOx/np-PtNi is obviously due to the higher electrocatalytic activity of np-PtNi towards H_2O_2 reduction. Moreover, np-PtNi with bimodal porosity, *i.e.*, big channels obtained from the removal of pure Al phase and nanopores obtained from the selective dealloying alloy phases, is more favorable for both GOx immobilization in the big channels and the free mass transfer of small molecules (*e.g.* substrates and products of GOx) through the nanopores. Note that the small nanopore size (4–6 nm) would be not possible for GOx (∼8 nm in diameter)[64] getting into the inner pore the nanorods.[65]

To evaluate the practical application of the np-PtNi-based biosensor, two real samples (liquor and glucose injection) were

tested. The results obtained with this biosensor are in good agreement with the values certified by the manufacturers (Table S1, ESI†) indicating that this biosensor is accurate for real sample determination.

Conclusions

By one-step dealloying PtNiAl alloy which contains multiphases, aligned np-PtNi nanorod-like structures were successfully prepared. These bimetallic nanorods with inherent nanoporous structure exhibit enhanced electrocatalytic activity towards ethanol oxidation and H_2O_2 oxidation/reduction compared with the commercial Pt/C catalyst, which can be used for sensitively sensing these two small molecules. When loaded with GOx, the GOx/np-PtNi biocomposite can be used for sensitive detection of glucose in a wide concentration range (0.5–21 mM). In addition to the enhanced catalytic activity and sensing performance, the nanoporous nanorod also has other advantages, such as easy preparation, improved precious metal utilization and suitability for large-scale preparation, *etc.* The novel nanoporous nanorods are not only scientifically interesting but also have great potential in electrochemical sensors and direct alcohol fuel cells.

Acknowledgements

References

1 A. C. Chen and P. Holt-Hindle, *Chem. Rev.*, 2010, **110**, 3767.
2 S. Chakraborty and C. R. Raj, *Biosens. Bioelectron.*, 2009, **24**, 3264.
3 Y. J. Zou, C. L. Xiang, L. X. Sun and F. Xu, *Biosens. Bioelectron.*, 2008, **23**, 1010.
4 S. Tang, X. Z. Wang, J. P. Lei, Z. Hu, S. Y. Deng and H. X. Ju, *Biosens. Bioelectron.*, 2010, **26**, 432.
5 K. W. Park, J. H. Choi, B. K. Kwon, S. A. Lee, Y. E. Sung, H. Y. Ha, S. A. Hong, H. Kim and A. Wieckowski, *J. Phys. Chem. B*, 2002, **106**, 1869.
6 T. Yajima, H. Uchida and M. Watanabe, *J. Phys. Chem. B*, 2004, **108**, 2654.
7 X. B. Ge, R. Y. Wang, P. P. Liu and Y. Ding, *Chem. Mater.*, 2007, **19**, 5827.
8 V. R. Stamenkovic, B. Fowler, B. S. Mun, G. F. Wang, P. N. Ross, C. A. Lucas and N. M. Markovic, *Science*, 2007, **315**, 493.
9 S. Koh, C. Yu, P. Mani, R. Srivastava and P. Strasser, *J. Power Sources*, 2007, **172**, 50.
10 C. M. Zhou, F. Peng, H. J. Wang, H. Yu, C. Peng and J. A. Yang, *Electrochem. Commun.*, 2010, **12**, 1210.
11 F. Liu, J. Y. Lee and W. J. Zhou, *J. Phys. Chem. B*, 2004, **108**, 17959.
12 J. Shui, C. Chen and J. C. M. Li, *Adv. Funct. Mater.*, 2011, **21**, 3357.
13 V. R. Stamenkovic, B. S. Mun, M. Arenz, K. J. J. Mayrhofer, C. A. Lucas, G. F. Wang, P. N. Ross and N. M. Markovic, *Nat. Mater.*, 2007, **6**, 241.
14 P. Strasser, S. Koh, T. Anniyev, J. Greeley, K. More, C. F. Yu, Z. C. Liu, S. Kaya, D. Nordlund, H. Ogasawara, M. F. Toney and A. Nilsson, *Nat. Chem.*, 2010, **2**, 454.
15 J. H. Zeng, H. L. Gao, S. J. Liao, Y. C. Xie and D. Dang, *Electrochim. Acta*, 2011, **56**, 2024.
16 J. X. Wang, H. Inada, L. Wu, Y. Zhu, Y. Choi, P. Liu, W. P. Zhou and R. R. Adzic, *J. Am. Chem. Soc.*, 2009, **131**, 17298.
17 S. S. Wong, C. Koenigsmann, A. C. Santulli, K. P. Gong, M. B. Vukmirovic, W. P. Zhou, E. Sutter and R. R. Adzic, *J. Am. Chem. Soc.*, 2011, **133**, 9783.
18 L. Xiao, B. Huang, L. Zhuang and J. Lu, *RSC Adv.*, 2011, **1**, 1358.
19 L. Wang and Y. Yamauchi, *Chem. Mater.*, 2011, **23**, 2457.

20 T. T. Trinh, D. Mott, N. T. K. Thanh and S. Maenosono, *RSC Adv.*, 2011, **1**, 100.

21 L. Wang, Y. Nemoto and Y. Yamauchi, *J. Am. Chem. Soc.*, 2011, **133**, 9674.

22 R. R. Adzic, M. B. Vukmirovic, J. Zhang, K. Sasaki, A. U. Nilekar, F. Uribe and M. Mavrikakis, *Electrochim. Acta*, 2007, **52**, 2257.

23 L. F. Liu, E. Pippel, R. Scholz and U. Gosele, *Nano Lett.*, 2009, **9**, 4352.

24 X. D. Li, J. Chen, F. Saeki, B. J. Wiley, H. Cang, M. J. Cobb, Z. Y. Li, L. Au, H. Zhang, M. B. Kimmey and Y. N. Xia, *Nano Lett.*, 2005, **5**, 473.

25 H. Qiu, Z. Zhang, X. Huang and Y. Qu, *ChemPhysChem*, 2011, **12**, 2118.

26 L. Y. Chen, J. S. Yu, T. Fujita and M. W. Chen, *Adv. Funct. Mater.*, 2009, **19**, 1221.

27 L. Zhang, X. Y. Lang, A. Hirata and M. W. Chen, *ACS Nano*, 2011, **5**, 4407.

28 X. H. Xia, W. Gao, J. J. Xu and H. Y. Chen, *J. Phys. Chem. C*, 2007, **111**, 12213.

29 H. Cui, Y. P. Dong and C. M. Wang, *J. Phys. Chem. B*, 2006, **110**, 18408.

30 P. C. Searson and C. X. Ji, *J. Phys. Chem. B*, 2003, **107**, 4494.

31 T. Y. Shin, S. H. Yoo and S. Park, *Chem. Mater.*, 2008, **20**, 5682.

32 R. Laocharoensuk, S. Sattayasamitsathit, J. Burdick, P. Kanatharana, P. Thavarungkul and J. Wang, *ACS Nano*, 2007, **1**, 403.

33 S. H. Yoo and S. Park, *Adv. Mater.*, 2007, **19**, 1612.

34 L. F. Liu, R. Scholz, E. Pippel and U. Gosele, *J. Mater. Chem.*, 2010, **20**, 5621.

35 Y. G. Sun and Y. N. Xia, *J. Am. Chem. Soc.*, 2004, **126**, 3892.

36 Y. Ding, Y. J. Kim and J. Erlebacher, *Adv. Mater.*, 2004, **16**, 1897.

37 H. J. Qiu, C. X. Xu, X. R. Huang, Y. Ding, Y. B. Qu and P. J. Gao, *J. Phys. Chem. C*, 2009, **113**, 2521.

38 C. Xu, Y. Liu, J. Wang, H. Geng and H. Qiu, *ACS Appl. Mater. Interfaces*, 2011, **3**, 4626.

39 Z. H. Zhang, Y. Wang, Z. Qi, W. H. Zhang, J. Y. Qin and J. Frenzel, *J. Phys. Chem. C*, 2009, **113**, 12629.

40 Z. H. Zhang, Y. Wang, Z. Qi, J. K. Lin and X. F. Bian, *J. Phys. Chem. C*, 2009, **113**, 1308.

41 R. Wang, C. Xu, X. Bi and Y. Ding, *Energy Environ. Sci.*, 2012, **5**, 5281.

42 Z. H. Zhang, Y. Wang, Z. Qi, C. Somsen, X. G. Wang and C. C. Zhao, *J. Mater. Chem.*, 2009, **19**, 6042.

43 H. J. Qiu, L. Y. Xue, G. L. Ji, G. P. Zhou, X. R. Huang, Y. B. Qu and P. J. Gao, *Biosens. Bioelectron.*, 2009, **24**, 3014.

44 H. J. Qiu, L. Lu, X. R. Huang, Z. H. Zhang and Y. B. Qu, *Bioresour. Technol.*, 2010, **101**, 9415.

45 J. T. Zhang, P. P. Liu, H. Y. Ma and Y. Ding, *J. Phys. Chem. C*, 2007, **111**, 10382.

46 Y. Ding and M. W. Chen, *MRS Bull.*, 2009, **34**, 569.

47 A. Wittstock, V. Zielasek, J. Biener, C. M. Friend and M. Baumer, *Science*, 2010, **327**, 319.

48 L. Y. Chen, T. Fujita, Y. Ding and M. W. Chen, *Adv. Funct. Mater.*, 2010, **20**, 2279.

49 H. J. Qiu and F. X. Zou, *ACS Appl. Mater. Interfaces*, 2012, DOI: 10.1021/am201659n.

50 J. F. Huang, *Chem. Commun.*, 2009, 1270.

51 J. Biener, G. W. Nyce, A. M. Hodge, M. M. Biener, A. V. Hamza and S. A. Maier, *Adv. Mater.*, 2008, **20**, 1211.

52 J. Snyder, T. Fujita, M. W. Chen and J. Erlebacher, *Nat. Mater.*, 2010, **9**, 904.

53 X. W. Zhou, R. H. Zhang, Z. Y. Zhou and S. G. Sun, *J. Power Sources*, 2011, **196**, 5844.

54 J. Erlebacher, M. J. Aziz, A. Karma, N. Dimitrov and K. Sieradzki, *Nature*, 2001, **410**, 450.

55 J. Erlebacher, *J. Electrochem. Soc.*, 2004, **151**, C614.

56 K. Sieradzki, *J. Electrochem. Soc.*, 1993, **140**, 2868.

57 J. Zhang, K. Sasaki, E. Sutter and R. R. Adzic, *Science*, 2007, **315**, 220.

58 S. N. Liu and C. X. Cai, *J. Electroanal. Chem.*, 2007, **602**, 103.

59 M. Zhou, Y. M. Zhai and S. J. Dong, *Anal. Chem.*, 2009, **81**, 5603.

60 H. J. Chen and S. J. Dong, *Biosens. Bioelectron.*, 2007, **22**, 1811.

61 J. Wang and M. Musameh, *Anal. Chem.*, 2003, **75**, 2075.

62 J. Wang, M. Musameh and Y. H. Lin, *J. Am. Chem. Soc.*, 2003, **125**, 2408.

63 K. B. Male, S. Hrapovic and J. H. T. Luong, *Analyst*, 2007, **132**, 1254.

64 H. J. Qiu, Y. Li, G. L. Ji, G. P. Zhou, X. R. Huang, Y. B. Qu and P. J. Gao, *Bioresour. Technol.*, 2009, **100**, 3837.

65 H. J. Qiu, C. X. Xu, X. R. Huang, Y. Ding, Y. B. Qu and P. J. Gao, *J. Phys. Chem. C*, 2008, **112**, 14781.